from 1978 to 1991 by E. Aguirre from the Museo Nacional de Ciencias Naturales, CSIC. Since 1992, the excavation and research of the Sierra de Atapuerca sites have been conducted by J. L. Arsuaga, J. M. Bermúdez de Castro, and E. Carbonell. The excavations are supported by the Junta de Castilla y León and the Research Project by the Ministerio de Educación y Ciencia (DGICYT, project no. PB93-0066-C03). The Atapuerca research carried out by the Archaeological Laboratory of Universitat Rovira i Virgili is included in the *Human Population Origins in the Circum-Mediterranean Area: Adaptations of the Hunter-Gatherer Groups to Environmental Modifications* project, which is supported by the European Union. Special thanks are given to the Laboratorio de Parasitología de la Facultad de Biología de la Universidad Complutense, which made research possible to J.L.A. Many individuals have contributed to this research effort (we are particularly grateful to A. Martín Nájera, C. Mallol, and J. Vallverdú). We are also grateful to J. Bischoff, F. Clark Howell, R. Klein, and T. White for comments on the manuscript.

14 March 1995; accepted 6 June 1995

Paleomagnetic Age for Hominid Fossils at Atapuerca Archaeological Site, Spain

Josep M. Parés* and Alfredo Pérez-González

A paleomagnetic investigation at the Gran Dolina site excavation (Atapuerca, Spain) shows that the sediments containing the recently discovered human occupation were deposited more than 780,000 years ago, near the time of the Matuyama-Brunhes boundary. Forty-one oriented samples were obtained from 22 sites along an 18-meter section of the Gran Dolina karst filling. The lower 16 sites displayed reversed-polarity magnetizations whereas the upper six sites were normal. The reversal spans the hominid finds at stratigraphic level TD6 (the Aurora stratum), and these hominid fossils are therefore the oldest in southern Europe.

Geomagnetic field directional changes resulting from secular variation and reversals of Earth's field have been successfully used to date Quaternary deposits in a variety of geological environments. The karst system of Atapuerca, located about 14 km east of the city of Burgos, Spain (Fig. 1), contains one of the largest, stratigraphically most complete Middle Pleistocene sequences (*1, 2*). A previous paleomagnetic study at the Gran Dolina stratigraphic section concluded that the Matuyama-Brunhes boundary was at the bottom of the series (*3*). The lithologies analyzed in that study consisted of red-yellow clays and silts. Most of the samples were demagnetized by the alternating field (AF) procedure and many of them yielded intermediate paleomagnetic directions. We therefore suspected that late remagnetization unresolved by AF demagnetization may be pervasive in those sediments. Consequently, we sampled the Gran Dolina section for paleomagnetic analysis (*4*). Our results imply that the boundary is higher in the section, at the near level of the discovered hominids and artifacts (*5*), and that these hominid fossils are therefore the oldest in southern Europe.

The lithostratigraphy of the Gran Dolina infilling has been divided into 11 levels (*1*).

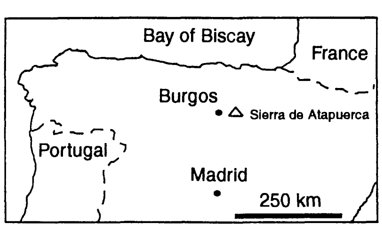

Fig. 1. Location of Sierra de Atapuerca, Spain.

The lowermost levels are composed of thin laminated brown (7,5YR5/4) silts (TD1) and clastic sediments of gravitational origin (TD2), covered by a thick speleothem. The overlying deposits (TD3/4 to TD11) are gravel and breccia. An accumulation of bat guano is also found at level TD9. The clasts consist of pebbles, cobbles, and occasionally boulders of limestone set in a matrix of brown (7,5YR5/6) to yellowish red (−5YR5/6) sandy silt. The clastic fragments come either from outside of the cave or from the walls. However, the sediments at level TD7 indicate a hydraulic regime. The top of the Gran Dolina series is marked by carbonated reddish yellow silty clays (7,5YR7/6) and terra rossa (2,5YR4/6). The horizon that yields hominid fossil remains (the Aurora stratum) is a massive red-brownish lutite bed 15 cm thick with dispersed fine clasts. The overall sedimentary package indicates local gravitational accumulation with some fluvial processes in the cavern.

The natural remanent magnetization (NRM) intensities (*6*) were 0.35 mA m^{-1} for the speleothems, 0.63 mA m^{-1} for the yellow clays, 7.0 mA m^{-1} for the bat guano, and up to 100 mA m^{-1} for the red clays. Progressive demagnetization revealed that the paleomagnetic samples from Gran Dolina are overprinted by a large secondary component. Thus most of the NRMs were carried by two components of magnetization; one of them was unblocked at demagnetization temperatures between 20° and 300°C with the present-day field direction, and the other was unblocked above 400°C in 45 of 50 specimens (Fig. 2). Some samples showed unstable magnetizations because of alteration and possible creation of superparamagnetic magnetite at high temperatures, as indicated by large increases in susceptibility. In these samples thermal demagnetization was terminated at 540°C because the magnetizations became too erratic. The low-temperature unblocking magnetizations are directed to the north with downward inclinations and conform to

Fig. 2. Representative Zijderveld demagnetization diagrams (*14*) of the Gran Dolina sediments. Sample numbers refer to the sampling sites in Fig. 4. Solid and open circles represent horizontal and vertical projections, respectively, onto the horizontal plane. Temperature steps are given in degrees Celsius for samples TDS6-1A, TDS7-1A, TDN13-2A, TDN15-2A, and TDN17-2A; alternating field steps are given in milliteslas for sample TDS3-2B. Temperature steps below 180° or 220°C are not shown in some samples to enhance the details at higher temperatures. NRM intensities are given in each diagram in milliamperes per meter.

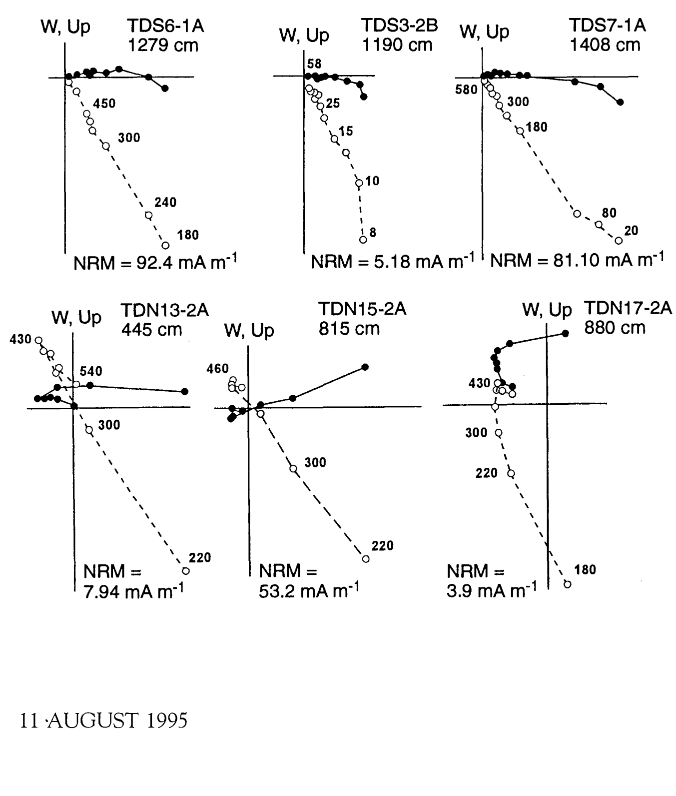

Earth's present field (Fig. 3A).

When AF demagnetization was applied to 10 specimens, in most cases the remanent magnetization was fully demagnetized by peak alternating fields of ~60 mT (Fig. 2). This analysis indicates that a low-coercivity phase dominates the remanence. Thermal treatment was preferable because it provided better resolution of the demagnetization trajectories. Comparison of magnetization component directions isolated by thermal and AF demagnetization suggests that the characteristic component is resolved over a relatively wide range of coercivities (20 to 60 mT) and unblocking temperatures (400° to 540°C). These observations are consistent with the isothermal remanent magnetization (IRM) acquisition curves, which are dominated by a low-coercivity phase (Fig. 3B). The most abundant magnetic mineral is magnetite, as interpreted from IRM diagrams. A slight rise in the IRM curves beyond 0.2 T was caused by a high-coercivity mineral; thermal demagnetization indicates that this mineral probably consists of iron oxyhydroxides in low concentration. A stable high-temperature component residing in magnetite is generally taken to be primary, although this mineral can also carry stable secondary magnetization in some geological environments (*7*). However, in a rock where the low-temperature component is normal and aligned with Earth's present field and the high-temperature component is reversed, the former is easily interpreted to represent a partial subrecent overprinting, whereas the latter can be considered a remanent magnetization that is older and most likely primary in age. In our samples, demagnetization trajectories that pointed to the origin on the orthogonal plots were considered as primary magnetizations.

Virtual geomagnetic pole (VGP) positions were calculated from the mean characteristic direction for each paleomagnetic site (Fig. 4 and Table 1). The VGP latitudes plotted against stratigraphic thickness resulted in a magnetic polarity reversal sequence for the section that shows two magnetozones, the bottom part being reversed. Archaeological and faunistic remains obviously constrain the section to be of Quaternary age [*Mimomys savini* zone, *Arvicola aff. sapidus* zone, and hominids (*5*)]. Previous ^{230}Th-^{234}U dating on levels that were correlated with archaeological level TD8 gave ages older than 0.35 Ma (*8*). Therefore, the observed magnetic polarity sequence must be Pleistocene in age and can be unambiguously correlated to the standard magnetic polarity time scale (*9*) (Fig. 4). The normal polarity magnetozone at the top of the Gran Dolina section corresponds to the Brunhes chron (Chron 1n) and the reversed-polarity zone corresponds to the Matuyama chron (Chron 1r). In southern Spain, it has also been recognized that Matuyama spans the *M. savini* zone (*10*) [*M. savini* at Gran Dolina spans stratigraphic levels TD3/4 to TD8 (Fig. 4); see table 1 of (*5*)].

The Matuyama chron contains several normal events of short duration. The youngest, Jaramillo (Chron 1r.1n), occurs between 1.07 and 0.99 Ma and therefore lasts 80,000 years (*11*). This normal event was not found in our magnetic stratigraphy because (i) the sampling interval was too widely spaced, (ii) there is a hiatus, or (iii) the sediments are younger than the age of the Jaramillo chron.

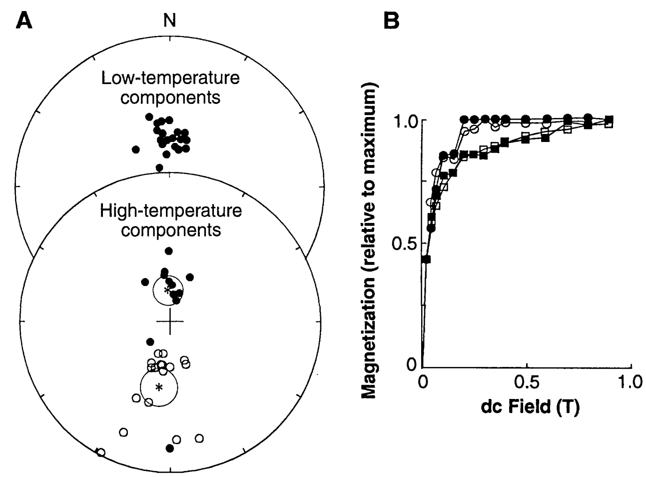

Fig. 3. (**A**) Equal-area projections of low- and high-temperature magnetization components. Each point represents a magnetization component of one specimen. Solid circles are projected onto the lower hemisphere; open circles are projected onto the upper hemisphere. Asterisks indicate the mean directions for the normal (mean declination D = 358°, inclination I = 66°, 95% confidence limit α_{95} = 11°) and reversed (D = 189°, I = −42°, α_{95} = 12°) high-temperature components. Statistics include only sites with VGP latitudes above 50° (Table 1). (**B**) Curves of IRM acquisition normalized to the peak magnetization for four representative samples.

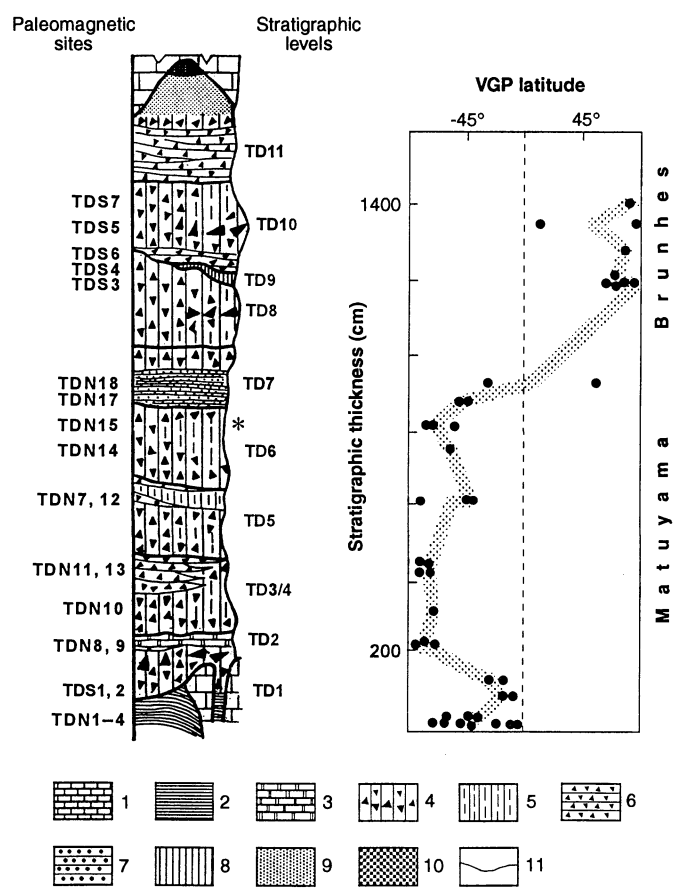

Fig. 4. Stratigraphy and corresponding paleomagnetic poles of the Gran Dolina section at Sierra de Atapuerca. Numbers to the left of the stratigraphic column refer to the paleomagnetic sampling sites; numbers to the right indicate the positions of the stratigraphic levels. An asterisk denotes the position of the Aurora stratum. VGP latitudes are plotted for each paleomagnetic site; the trace of the path is determined by the Fisherian (*15*) VGP mean direction for each sampling site. Key to stratigraphic column: 1, limestone and dolomite; 2, very thin laminated silt-clay; 3, speleothem; 4, sandy mudstone angular clast-supported breccias; 5, sandy mudstone; 6, stratified clast-supported fine-grain gravels, eventually with matrix; 7, cross-bedded calcarenites; 8, bat guano; 9, silty clay; 10, terra rossa; and 11, main stratigraphic discontinuities.

J. M. Parés, Institut de Ciències de la Terra "Jaume Almera," Consejo Superior de Investigaciones Científicas (CSIC), Martí i Franquès sin número, 08028 Barcelona, Spain.
A. Pérez-González, Centro de Ciencias Medioambientales, CSIC, Serrano 115, 28006 Madrid, Spain.

*Present address: Department of Geological Sciences, University of Michigan, 1006 C. C. Little Building, Ann Arbor, MI 48109–1063, USA.

Table 1. Paleomagnetic results by site. The positions of paleomagnetic sites are indicated in centimeters (Fig. 4). Sites are classified according to Johnson's system (*16*): class 1 if precision parameter *k* (*15*) was greater than 10, class 2 if *k* was less than 10, and class 3 if one specimen was used.

Site	Height (cm)	Mean declination (degrees)	Inclination (degrees)	VGP latitude (degrees)	VGP longitude (degrees E)	Class	Lithology
TDS7	1408	353	55	81	218	1	Red silt
TDS5	1352	311	79	53	329	2	Red silt
TDS6	1279	9	69	78	24	3	Red silt
TDS4	1205	25	54	69	100	3	Red silt
TDS3	1190	358	66	84	344	1	Bat guano
TDN18	930	130	61	6	31	2	Carbonated silt
TDN17	880	184	−14	−55	350	1	Carbonated silt
TDN15	815	168	−44	−71	31	2	Carbonated silt
TDN14	750	204	−32	−58	310	3	Red silt
TDN12	617	250	−71	−44	225	3	Red silt
TDN7	615	202	−29	−57	315	2	Red silt
TDN13	445	196	−65	−78	239	1	Red silt
TDN11	435	195	−55	−76	292	1	Red sandy silt
TDN10	320	202	−53	−71	286	3	Red sandy silt
TDN8	235	196	−55	−76	290	1	Speleothem
TDN9	230	180	−56	−84	356	3	Speleothem
TDS2	150	250	−23	−23	271	1	Yellow silt
TDS1	110	108	−2	−14	75	1	Yellow silt
TDN4	35	233	−29	−37	280	3	Red clay
TDN2	30	187	−11	−53	345	2	Red clay
TDN1	17	264	−56	−28	240	2	Red clay
TDN3	15	250	−56	−37	248	2	Red clay

Unconformities are likely in karst environments. On the other hand, we cannot rule out the possibility that the Gran Dolina sediments with reverse magnetization are younger than Jaramillo. If that is the case, then a rough sedimentation rate of about 50 cm per 1000 years is indicated; this value is consistent with the rates of deposition found in other cave sediments (*12*). The stratigraphic level TD6, and hence the Aurora stratum, is located within Matuyama and therefore is older than 0.78 Ma.

REFERENCES AND NOTES

1. E. Carbonell and X. P. Rodriguez, *J. Hum. Evol.* **26**, 291 (1994).
2. J.-L. Arsuaga, I. Martínez, A. Gracia, J.-M. Carretero, E. Carbonell, *Nature* **362**, 534 (1993) and references therein.
3. J. C. Carracedo, F. Heller, V. Soler, E. Aguirre, in (*13*), pp. 193–199.
4. Clay and silt deposits are sufficiently soft and contain an appreciable amount of water such that samples were obtained by simply hammering a brass tube with a stainless steel reinforced tip that was pushed into the cleaned outcrop surface at any desired angle. A standard orientation device (compass-inclinometer) was used to measure the azimuth and dip of the obtained cylinders in situ. Sediment samples were stored in cylindrical plastic boxes and were impregnated with a water solution of sodium silicate (1:1) to prevent further distortion. For harder deposits (lithified siltstones and speleothems), a portable drill fitted with a diamond coring bit (diameter 2.5 cm) was used to obtain the samples in the field.
5. E. Carbonell *et al.*, *Science* **269**, 826 (1995).
6. Magnetization measurements were made on a GM400 three-axis SQUID magnetometer housed in a three-pair Helmholtz coil at CSIC in Barcelona. The noise level of this magnetometer is 7×10^{-3} mA m^{-1}, well below the magnetization intensity of the measured samples. Least-squares fits to the linear demagnetization trajectories for both the low- and high-temperature components in each sample were made by principal components analysis [J. L. Kirschvink, *Geophys. J. R. Astron. Soc.* **62**, 699 (1980)].
7. D. Suk, D. R. Peacor, R. Van der Voo, *Nature* **345**, 611 (1990).
8. R. Grun and E. Aguirre, in (*13*), pp. 201–204.
9. S. C. Cande and D. Kent, *J. Geophys. Res.* **97**, 13917 (1992).
10. O. Oms *et al.*, *Phys. Earth Planet. Inter.* **85**, 173 (1994).
11. J.-P. Valet and L. Meynadier, *Nature* **366**, 234 (1993).
12. V. A. Schmidt, *Science* **217**, 827 (1982); R. Lovlie, K. L. Ellingsen, S.-E. Lauritzen, *Geophys. J. Int.* **120**, 499 (1995).
13. E. Aguirre, E. Carbonell, J. M. Bermúdez de Castro, Eds., *El hombre fósil de Ibeas y el Pleistoceno de la Sierra de Atapuerca* (Junta de Castilla y León, Valladolid, Spain, 1987).
14. J. D. A. Zijderveld, in *Methods in Palaeomagnetism*, D. W. Collinson, K. M. Creer, S. K. Runcorn, Eds. (Elsevier, Amsterdam, 1967), pp. 254–286.
15. R. A. Fisher, *Proc. R. Soc. London Ser. A* **217**, 295 (1953).
16. N. M. Johnson *et al.*, *J. Geol.* **93**, 27 (1985).

17. We thank J. Bischoff, W. J. Glen, W. Farrand, J. Stamatakos, R. Van der Voo, and two anonymous reviewers for discussion and J. Dinarès and A. Gómez for laboratory assistance. The excavations were supported by funds from Dirección General de Investigación Científica y Técnica (DGICYT; project PB93066C3-03) and Junta de Castilla y León. Laboratory measurements were supported in part by DGICYT (project PB91-0096).

14 March 1995; accepted 30 May 1995

Functional Significance of Symmetrical Versus Asymmetrical GroEL-GroES Chaperonin Complexes

Andreas Engel,* Manajit K. Hayer-Hartl, Kenneth N. Goldie, Günter Pfeifer, Reiner Hegerl, Shirley Müller, Ana C. R. da Silva, Wolfgang Baumeister, F. Ulrich Hartl

The *Escherichia coli* chaperonin GroEL and its regulator GroES are thought to mediate adenosine triphosphate–dependent protein folding as an asymmetrical complex, with substrate protein bound within the GroEL cylinder. In contrast, a symmetrical complex formed between one GroEL and two GroES oligomers, with substrate protein binding to the outer surface of GroEL, was recently proposed to be the functional chaperonin unit. Electron microscopic and biochemical analyses have now shown that unphysiologically high magnesium concentrations and increased pH are required to assemble symmetrical complexes, the formation of which precludes the association of unfolded polypeptide. Thus, the functional significance of GroEL:$(GroES)_2$ particles remains to be demonstrated.

Chaperonins mediate the adenosine triphosphate (ATP)–dependent folding of newly synthesized proteins in the cytosol, in mitochondria, and in chloroplasts (*1*), preventing off-pathway steps during folding that result in aggregation. This function is intimately connected with the characteristic oligomeric structure of chaperonins, which has been analyzed by electron microscopy (*2–5*) and x-ray crystallography (*6*). The chaperonin of *E. coli*, GroEL, is composed of 14 subunits that are arranged in two heptameric rings stacked back-to-back, resulting in a cylindrical structure enclosing a central cavity. Three domains are distinguishable in the 58-kD subunit (*6*): (i) an equatorial domain that mediates the contact between the rings and contains the ATP binding site, (ii) an apical domain that forms the opening of the central cavity, and (iii) an intermediate, hinge domain. Electron microscopic data

A. Engel, K. N. Goldie, S. Müller, Maurice E. Müller Institute, Biozentrum, University of Basel, CH-4056 Basel, Switzerland.
M. K. Hayer-Hartl, A. C. R. Silva, F. U. Hartl, Howard Hughes Medical Institute and Cellular Biochemistry and Biophysics Program, Memorial Sloan-Kettering Cancer Center, New York, NY 10021, USA.
G. Pfeifer, R. Hegerl, W. Baumeister, Max Planck Institut für Biochemie, D-82150 Martinsried, Germany.

*To whom correspondence should be addressed.